Hindawi Publishing Corporation
International Journal of Rotating Machinery
Volume 2015, Article ID 641601, 14 pages
http://dx.doi.org/10.1155/2015/641601

Research Article

Experimental Investigation of Stall Inception Mechanisms of Low Speed Contra Rotating Axial Flow Fan Stage

Tegegn Dejene Toge and A. M. Pradeep

Department of Aerospace Engineering, Indian Institute of Technology Bombay, Powai, Mumbai 400 076, India

Correspondence should be addressed to A. M. Pradeep; ampradeep@aero.iitb.ac.in

Received 29 June 2015; Accepted 31 August 2015

Academic Editor: Alessandro Corsini

The present paper is an attempt in understanding the stall inception mechanism in a low speed, contra rotating axial flow fan stage, using wavelet transforms. The rotors used in this study have relatively large tip gap (about 3% of the blade span) and aspect ratio of 3. The study was carried out near stall and at stall mass flow conditions for different speed ratios of rotor-2 to rotor-1. Unsteady pressure data from the casing wall mounted sensors are used to understand the stall inception mechanism. The wavelet transform clearly indicates that stall inception occurs mainly through long length scale disturbances for both rotors. It also reveals that short length disturbances occur simultaneously or intermittently in the case of rotor-1. The analysis shows the presence of a strong modal disturbance with 25–80% of the rotor frequency in the case of rotor-1 at the stall mass flow for all the speed combinations studied. The most interesting thing observed in the present study is that the frequency amplitude of the disturbance level is very small for both rotors.

1. Introduction

Contra rotating turbomachines have several advantages like improved flow capacity, compact size, and higher aerodynamic performance in both ducted and unducted configurations. This type of turbomachines differs from the conventional turbomachines in that there is no stator between two rotating rows of blades. Recovering static pressure from the outflow of the front rotor and direct transfer of energy to the working fluid are the two main contributions of the rear rotor [1]. Preliminary studies by different researchers have shown that the contra rotating machines are known to provide much better off-design performance and there is a possibility of increasing the operating range of compressors and fans [2–4].

Aerodynamic instabilities like rotating stall and surge are the major issues associated with axial flow compressors and fans. Achieving wider and stable operating range is a very important design parameter in the design exercise. To achieve such a compressor/fan design, a thorough understanding of the stall inception mechanism is necessary. Numerous investigations have been performed by various researchers on the stall inception mechanism of axial flow compressors or fans and a promising progress is seen in understanding the unsteady flow phenomena. Modal waves and spikes are the two main known stall inception patterns or stall precursors so far identified [5, 6]. Modal waves (long length scale disturbances) are gradual and progressive type of stall inception with a small amplitude and low frequency disturbance, which propagates at approximately 20–45% of a rotor speed and increases to 40–60% when it grows to fully develop rotating stall [7]. Camp and Day [8] have identified the spike type short length scale disturbance, which rotates at 70–80% of the rotor speed and originates near tip region because of tip vortices. Vo et al. [9] tried to explain the two criteria of spike type stall disturbances, namely, leading edge spillage and trailing edge back flow near stall mass flow condition. The findings are perceived as important contribution in the understanding of the spike type stall inception in axial flow compressors. Recently, Taghavi-Zenouz and Abbasi [10] observed the same phenomena from their numerical investigation of multiple spike stall cell in low speed axial flow rotor blade row. Spike and modal inceptions may appear simultaneously in some cases and this indicates that they are distinct but not exclusive. Pismenny and Levy [11] carried out a theoretical investigation

of the pressure signal which included spike and oscillating modes and they have proved the existence of modal type and spike type of stall inception. Lin et al. [12] have observed intermittent pattern of spike evolution in low speed axial flow compressor. In addition to modal waves and spike disturbances, Day et al. [13] and recently He et al. [14] identified shaft order perturbations. These perturbations, which are present in all the compressors, are mainly caused by nonuniform tip clearance and eccentricity of the rotor and the casing.

Researchers have been using different methods of unsteady pressure and velocity signal analysis for stall detection. Visual inspection of the time series, spatial Fourier decomposition, traveling wave energy, wavelet transform, and a windowed spatial correlation function are some of the methods used for stall detection of unsteady pressure signal [15]. Wavelet transform is a promising method to obtain the time frequency energy distribution of a signal. Wavelet transforms help in detecting the inception of stall and its evolution process [16]. In the recent past, continuous wavelet transform with Morlet wavelet has gotten significant attention in the unsteady pressure signal analysis for stall detection. Even though wavelet transform gives good localization in time and frequency domain, the interpretation of the wavelet spectrogram is difficult and there is no clear guide line in choosing the wavelet bases, the set of discrete scales, and time for performing a continuous wavelet transform computation [12]. Lin et al. [12], Ziach et al. [17], Salunkhe and Pradeep [18], and He et al. [14] have used the wavelet transform to detect the stall inception in low speed axial flow compressors/fans. It can be seen from their investigation that the wavelet transform is a promising tool to detect the stall onset and its propagation.

From the above literature, it is evident that contra rotating turbomachines have immense potential. However, to realize this promising technology, it is necessary that the fundamental flow physics especially those associated with stall inception should be well understood. There is limited published literature on the stall inception mechanism in a contra rotating axial fan/compressor. Experimental and numerical simulations done by Sharma et al. [19], Wang et al. [20], and Gao et al. [21] are some of the published work in the field of a stall inception mechanism study of contra rotating compressors. The simulation result of Gao et al. [21] shows that rotor-1 is the first stage of the contra rotating compressors to stall depending upon the tip clearance. For tip clearance greater than 0.5 mm, rotor-1 stalls first, whereas, for tip clearance less than 0.5 mm, rotor-2 stalls first. It was attempted to relate the tip clearance size with the first stall stage based on the slope of the pressure curve. Sharma et al. [19] have indicated that the front rotor will not stall when the rear rotor rotates at speed fifty percent higher than the front rotor. Mistry and Pradeep [2] have shown in their study that the rotor-2 goes to stall before rotor-1 at near stall mass flow condition. However, the above studies have limited flow physics associated with the stall inception of a contra rotating fan stage. Hence, the present study aims to understand the stall inception mechanism and its propagation of low subsonic, high aspect ratio, contra rotating fan stage. It is also intended to identify the peculiar stall triggering mechanism using the wavelet analysis for adequate representation of time and frequency of acquired unsteady pressure signals.

2. Experimental Setup and Instrumentation

2.1. Experimental Setup. The experimental test rig used in this study is a low subsonic speed contra rotating axial flow fan (CRAF) stage at the Indian Institute of Technology Bombay (Figure 1(a)). The CRAF consists of two rotors (rotor-1 and rotor-2) that rotate in the opposite direction. Two AC induction motors of 15 kW each drive the two rotors with separate variable frequency drives (VFD). The VFD also has a provision to measure and display the power consumed by the motors. A bellmouth at the front of the rig is used for smooth flow of air into the test section and a throttle cone at the exit of the setup is used to control the mass flow rate. The rotors are designed for a total mass flow of 6 kg/s and rotational speed of 2400 RPM for both rotors. The nominal tip gap is 3.5 mm for both rotors. The number of blades is 19 and 17 for rotor-1 and rotor-2, respectively, and both rotors have a chord length of 45 mm. Further description of the experimental rig can be obtained from Mistry and Pradeep [2] and hence not being reproduced here for brevity. Circumferentially arranged high response dynamic pressure sensors on the casing wall shown in Figure 1(b) are used for unsteady pressure measurement and stall inception studies.

2.2. Instrumentation. High response pressure sensors (ET 3DC-312M-1D, from M/s Kulite Semiconductor Products, Inc., USA) are used for measuring the unsteady pressure fluctuations. Four pressure sensors are arranged circumferentially near the leading edge of rotor-1 and rotor-2 on the casing wall of the test section (Figure 1(b)). The measurement range and sensitivity of these sensors are (0-1) PSI and 2508.93 mV/PSI, respectively. Data is acquired using a 16-bit resolution A/D board (NI 6040E) at a sampling frequency of 10 kHz and low pass filtered with fifth-order Butterworth filter for attenuation of frequencies higher than the cut-off frequency.

2.3. Experimental Data Procedure. Unsteady pressure traces are acquired at three different operating conditions, namely, design, peak pressure, and stall mass flow conditions. For a given operating point it is ensured that the transient effects of the throttle valve motion do not interfere with data acquisition. Data was acquired over a minimum duration of 30 s, which corresponds to 1200 or greater rotor revolutions. The time variant data is digitized using National Instruments A/D modules (through LabVIEW) with each channel being sampled at 10 kHz.

3. Methodology of Dynamic Signal Analysis

Circumferentially arranged fast response pressure sensors for different mass flow and speed conditions capture the raw pressure-time signals. For given speed combination of the rotors say design speed of 2400-2400 RPM, the mass flow is varied from point "A" to point "B" indicated in Figure 2. By changing the throttle cone position, the raw data is

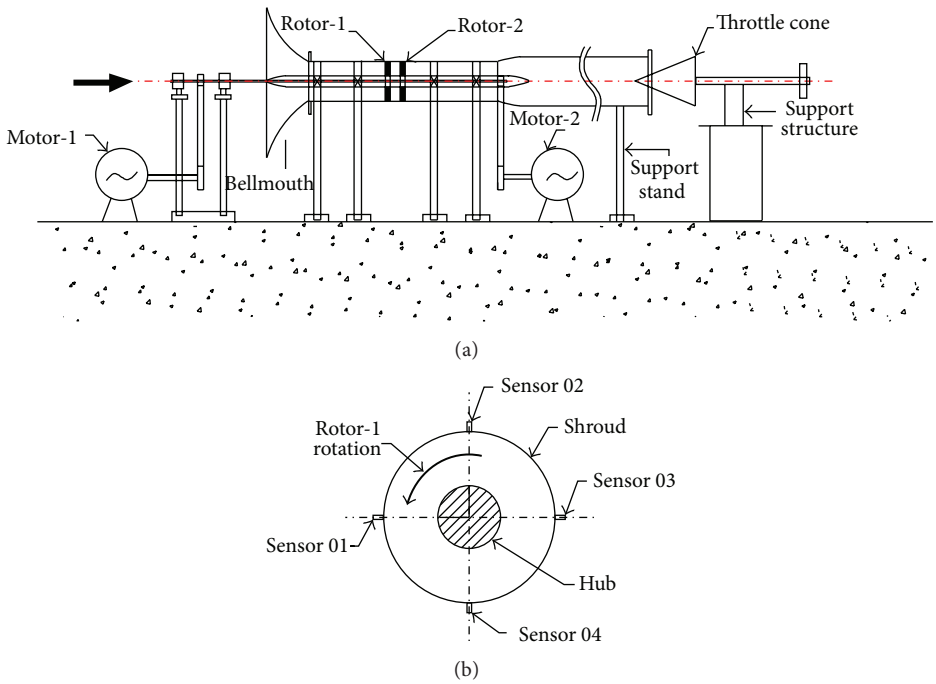

FIGURE 1: (a) Schematic of experimental rig. (b) Circumferential location of the unsteady pressure sensors (front view).

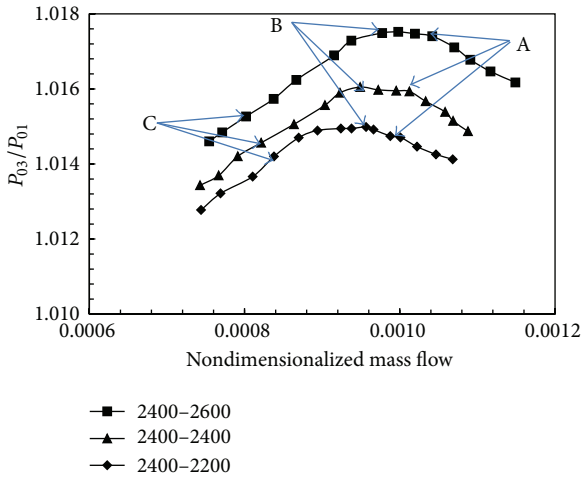

FIGURE 2: Performance characteristics at different speed combinations.

recorded for each mass flow condition. For off-design speed combination, the same procedure is followed to obtain the required data.

The acquired unsteady data from the Kulite sensors are postprocessed by using wavelet transform, which gives good localization in time and frequency domain. A code for this is developed in MATLAB for one-dimensional continuous Morlet wavelet transform. The continuous, nonorthogonal complex valued wavelet is the best choice to determine breakdown points in the rotating flows as the discrete wavelet transform may skip the breakdown point during its step interval [12]. The Morlet mother wavelet is given by the following equation:

$$\Psi_0(\eta) = \pi^{-1/4} e^{i\omega_0\eta} e^{-\eta^2/2}. \quad (1)$$

The wavelet coefficients can be determined by the following equation, as reported by Torrence and Compo [22]:

$$W_n(s) \sum_{k=0}^{N-1} \hat{x}_k \hat{\psi}(s\omega_k) e^{i2\pi kn/N}, \quad (2)$$

where Ψ_0 is a function of the mother wavelet, η is the nondimensional time, W is the wavelet coefficient, x is the time series, k is the frequency index, s is the scale, N is the total number of points, $\hat{}$ denotes the Fourier transform of the corresponding parameter, and $n = 0, \ldots, N-1$.

The above wavelet coefficients are then multiplied by a suitable factor to have unit energy. The advantage of Morlet wavelet is that the center frequency ω_0 can be varied to vary the individual localization in time and frequency domains. The lower values of ω_0 correspond to greater time resolution and higher values represent greater frequency resolution. For transient rotating flows, $\omega_0 = 6$ results in sufficient localization in time as well as frequency domain, as reported by Farge [23] and Lin et al. [12]. Hence, $\omega_0 = 6$ is used for all the wavelet transforms in the present paper.

4. Results and Discussions

The present study on stall inception mainly focuses on the stall behavior at near stall mass flow and stall mass flow conditions for different speed combinations of rotor-1 and rotor-2. The overall performance map for the three speed

combinations of the CRAF stage is shown in Figure 2 and the corresponding design mass flow (point A), near stall mass flow (point B), and stall mass flow (point C) points are indicted in the figure.

Based on the experience gained from the steady measurement of performance data [2], the maximum data recording time is kept as 45 s. At the stall mass flow, the duration is reduced to 10–15 s, since prolonged operation after initiation of stall may result in mechanical failure of the system. Even though the data is captured for the three mass flow conditions (design, near stall, and stall mass flow), the present paper mainly discusses near stall flow and stall mass flow conditions for three speed combinations. Wavelet and time pressure analysis of a datum case, with the fans at design mass flow and design speeds, is also discussed for reference purpose. The onset of stall and its propagation through the two rotors (rotor-1 and rotor-2) is discussed in the following paragraphs.

4.1. Stall Inception Study of Rotor-1. Several researchers have tried to understand the stall behavior of rotor-1 of a contra rotating compressor/fan stage. Sharma et al. [19] have indicated that the front rotor will not stall when the rear rotor rotates at speed fifty percent higher. Roy et al. [4] and Mistry and Pradeep [2] have also indicated in their respective studies that operating the second rotor at higher rotational speed improves the performance and the stable operating range of the stage. Wang et al. [20] have shown in their study that rotor-1 is the first stall stage if the tip clearance size is greater than 0.5 mm. Recently, Wang et al. [24] have shown in their numerical study that the performance and stability of the upstream rotor are highly affected for large tip clearance size of the stage. In the present case, greater attention is given for rotor-1 since the CRAF stage was designed with a larger tip gap. In the subsequent paragraphs, the stall inception and its propagation of rotor-1 for different speed combinations will be discussed.

It is well known that the rotational speed of a rotor can affect the stall onset and its propagation. The numerical simulation by Choi et al. [25] has shown that stall cell size is proportional to fan speed size; that is, when the speed increases, the size of the stall cell also increases. In a CRAF, the speed of each rotor plays a major role in the performance. Gao et al. [21] in their numerical investigation of contra rotating compressors indicated that the stall onset of the two rotors depends on their speed ratio. In the present investigation, experiments are carried out for three speed combinations: 2400-2400 RPM (design speed), 2400–2200 RPM, and 2400–2600 RPM of rotor-1 and rotor-2, respectively. In all the speed combinations, the first rotor rotation is kept constant at the design speed and the speed of the second rotor is varied. This is because the speed of the second rotor is known to significantly affect the overall performance of the CRAF stage. In the following subsections, the experimental results of the unsteady casing wall static pressure data for peak pressure and stall mass flow conditions at a design speed will be discussed.

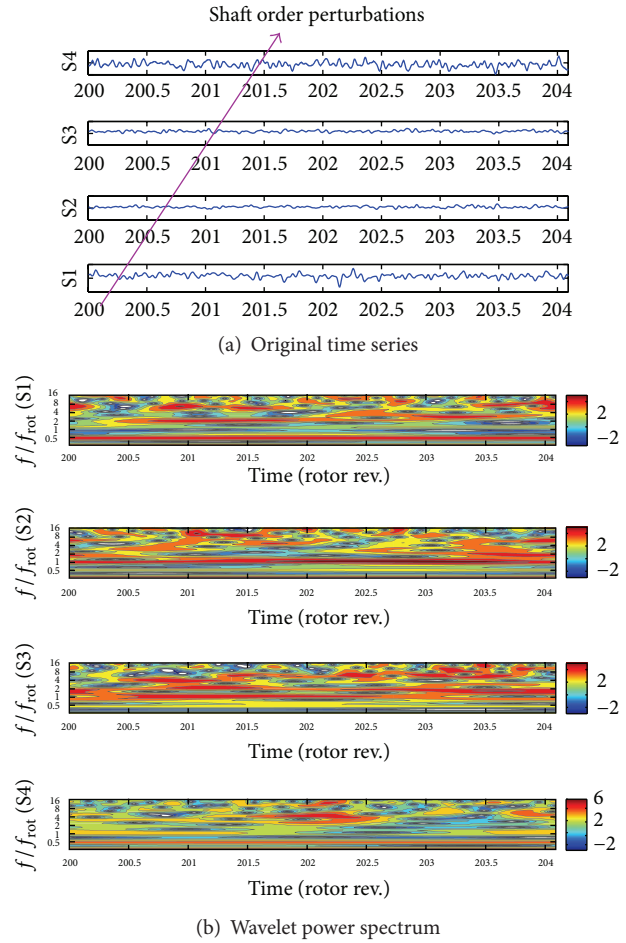

(b) Wavelet power spectrum

Figure 3: Wavelet analysis of unsteady data segment of four sensors of rotor-1 at design mass flow (point A) for design speed combination.

4.1.1. Design Mass Flow Condition. The wavelet transforms of unsteady data of casing wall static pressure of rotor-2 at design mass flow and design speed combination are shown in Figure 3. It is intended to show how the rotor behaves at design mass flow or far from stall mass flow. In this case small disturbances like shaft order perturbations are observed and sensor 3 captured LLSD which propagate with 0.5 times the rotor frequency.

4.1.2. Peak Pressure or Near Stall Mass Flow Condition. The peak pressure mass flow condition is the point at which the compressor/fan operates at the maximum pressure. This operating point is also a very critical point since there is an imminent threat of compressor/fan stall. The accurate prediction of this point is therefore very important. The stall margin will be decided for safe and stable operation based on this point. The peak pressure mass flow point (point A in Figure 2) was determined during the flow characterization study of CRAF stage conducted by Mistry and Pradeep [2].

Figure 4 shows the unsteady pressure trace and the wavelet power spectrum of four sensors at the leading edge of rotor-1 for the design speed. The corresponding pressure

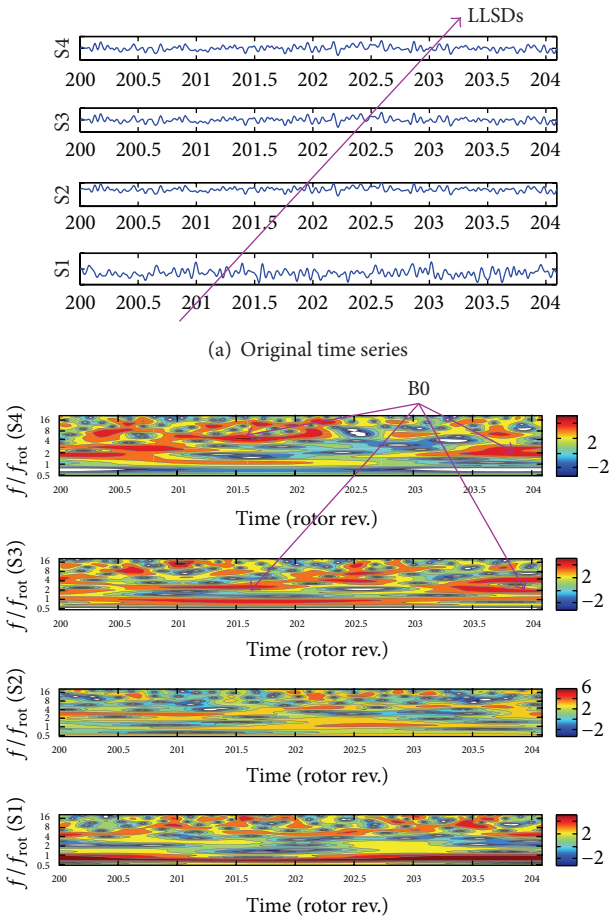

FIGURE 4: Wavelet analysis of unsteady data segment of four sensors of rotor-1 at near stall mass flow (point B) for design speed combination.

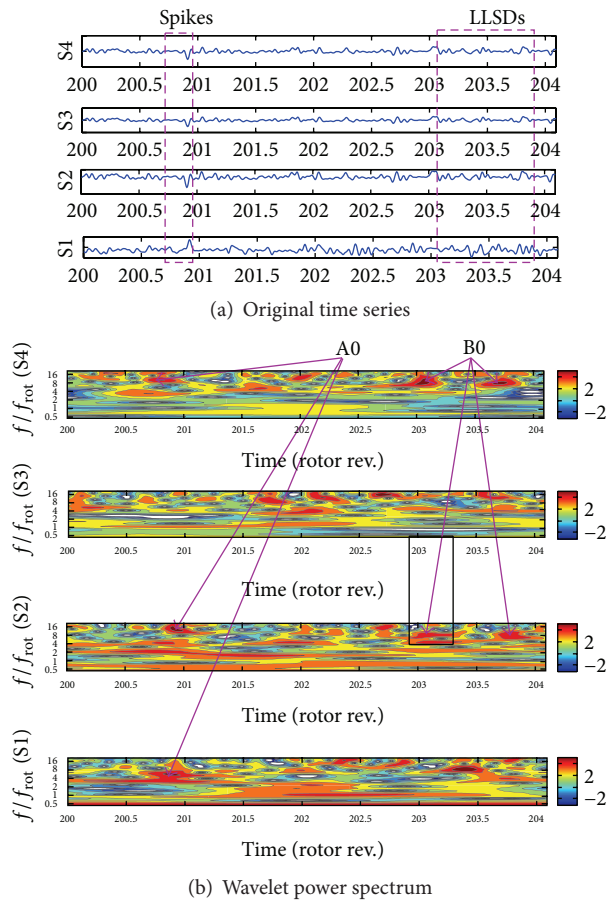

FIGURE 5: Wavelet analysis of unsteady data segment of four sensors of rotor-1 at near stall mass flow (point B) for speed combination of 2400–2200 RPM.

trace and the wavelet power spectrum for the off-design speed are shown in Figure 5. From the original time series data, the presence of long length scale disturbance (LLSD) with emerging spikes for both speed combinations can be observed. The wavelet power spectrum in Figures 4(b) and 5(b) also indicates the presence of LLSDs (indicated with "B0") and spikes (indicated with "A0"). The modal wave disturbance rotates around 50% of the rotor frequency. The unsteady pressure trace and wavelet power spectrum of 2400–2600 RPM at the same mass flow condition show similar behavior (figure is not shown for brevity). The same phenomenon was reported by Nishioka [26] for stall inception pattern of a low stagger, large tip clearance axial fan. For further understanding of the stall behavior, Figure 6 shows the wavelet analysis on the data segment from 200 to 204 rotor revolutions of one of the sensors from Figure 5. Figures 6(a)–6(d) show the original time series, the wavelet power spectrum, the global power spectrum, and the Fourier power spectrum, respectively. The global power spectrum represents the averaged power distribution over the frequency range. The Fourier power spectrum is computed by taking the FFT of time series data segment and then squaring it in log2 scale. The abscissa and ordinate of Figure 6(b) are time in terms of rotor revolutions and frequency nondimensionalized by the rotor frequency, respectively. Wavelet energy spectrogram enables detection and tracking of the disturbances generated during stall evolution process. An increase in the local flow disturbance is indicated by rectangular boxes for different frequency levels in Figure 6(b) of wavelet power spectrum. The two dashed rectangles show the LLSD which rotate with 1 to 16 times the rotor frequency and the small size solid rectangle shows the emerging spike type disturbance with frequency of 3 to 8 times the rotor frequency. The mild modal wave with 50% of the rotor frequency is indicated by "A1" in the wavelet power spectrum and Fourier power spectrum.

4.1.3. Stall Mass Flow Condition. After the initial disturbance of the flow at peak mass flow or near stall mass flow, the CRAF stage goes into deep stall zone and the condition and the type of stall determine the stability of the system. In order to capture the stall in the stall region, data is captured with shorter intervals of throttling to avoid sudden surge, which may cause mechanical damage or failure of the test rig. In this region, the flow behavior through the compressor/fan is

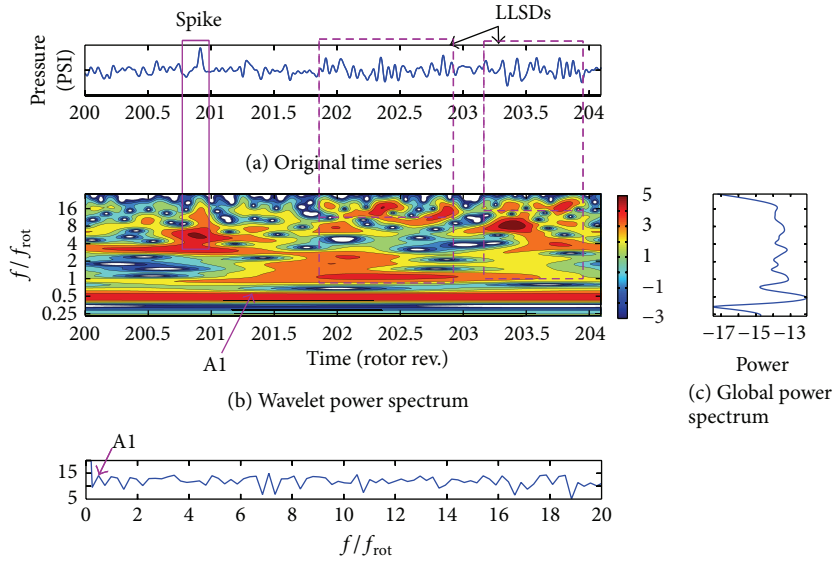

FIGURE 6: Wavelet analysis of unsteady data segment of one of the sensors of rotor-1 at near stall mass flow (point B) for speed combination of 2400–2200 RPM.

highly unsteady. The stall point (point B) at which data was recorded is indicated in Figure 2 for the design and off-design speed combinations.

Figure 7 shows the unsteady pressure traces and wavelet power spectrum at the stall mass flow for design speed combination. It is observed that long length scale disturbances are captured by one of the sensors after 943 rotor revolutions and they diminish at around 945 rotor revolutions. Except small fluctuations in pressure the other three sensors have not captured any stall phenomena. Detailed wavelet analysis of unsteady pressure measurement data obtained from pressure sensor 1 is given in Figure 8. The spikes with small amplitude and low wavelet energy spot are indicated by the small size solid line rectangular boxes and the LLSDs are indicated with larger size dashed line rectangular boxes in Figures 8(a) and 8(b). A strong modal wave, which propagates 25% to 50% of the rotor frequency, is indicated in Figures 8(b) and 8(d). This shows that LLSD is the dominant type of disturbance during onset of the stall. The length scale of LLSD disturbance is about one rotor revolution.

In order to understand the progress or decay of the stall cell, the wavelet power spectra of the data segment from 1164 to 1172 rotor revolutions are depicted in Figure 9. It is observed that the stall cell grows in disturbance energy and amplitude. The dashed rectangle is shown to identify the LLSDs. In this, it can be seen that LLSDs (indicated with "C2") and SLSDs or spikes (indicated with "A2") occur simultaneously. The LLSDs propagate with 2 to 4 times the rotor frequency and the SLSDs propagate in some cases 4 to 16 times the rotor frequency and in other cases they propagate 8 to 16 times the rotor frequency.

Figure 10 shows the pressure versus time trace and the corresponding wavelet power spectrum of data segment from 400 to 408 rotor revolutions at the speed combination of

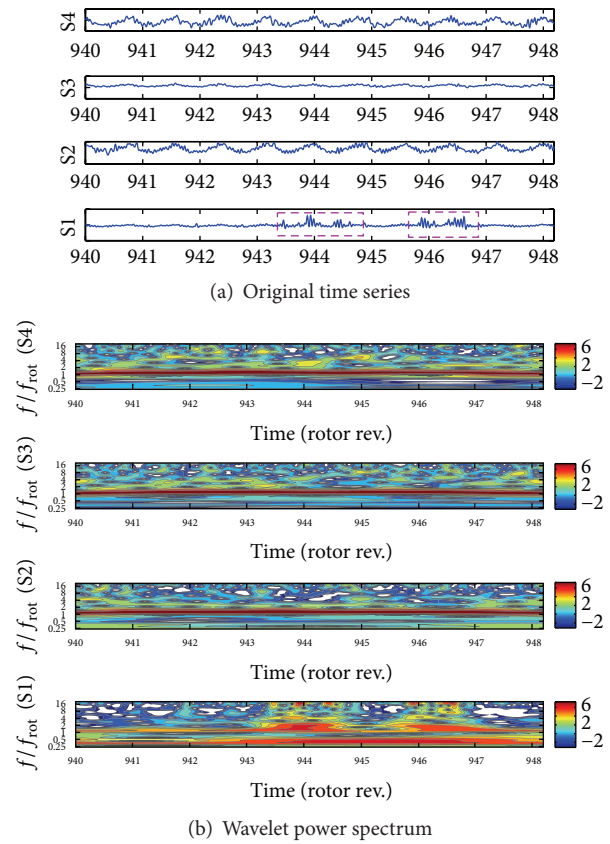

FIGURE 7: Wavelet analysis of unsteady data segment of four sensors of rotor-1 at stall mass flow (point C) for design speed combination.

2400–2200 RPM for all the four sensors. The presence of high energy level pressure disturbance for all the sensors is evident. Here, the evolution of the stall cell is through long

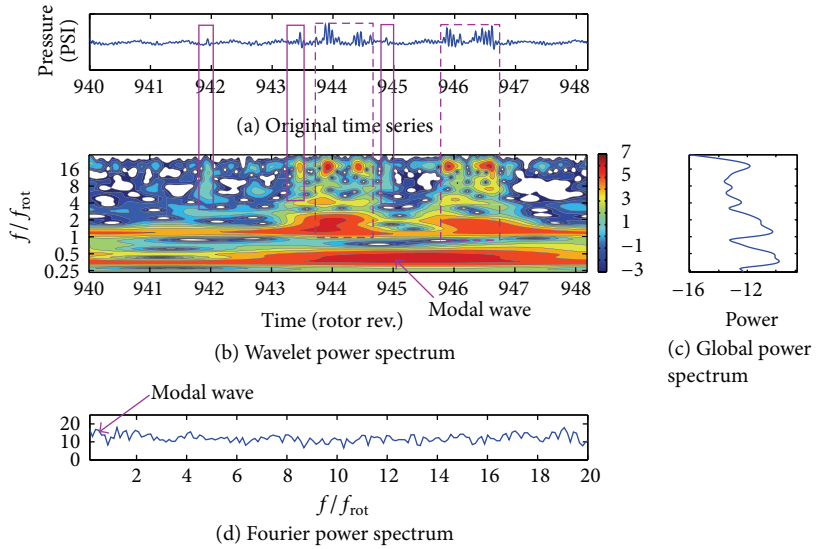

FIGURE 8: Wavelet analysis of data segment for sensor 1 of rotor-1 at stall mass flow (point C) for design speed combination.

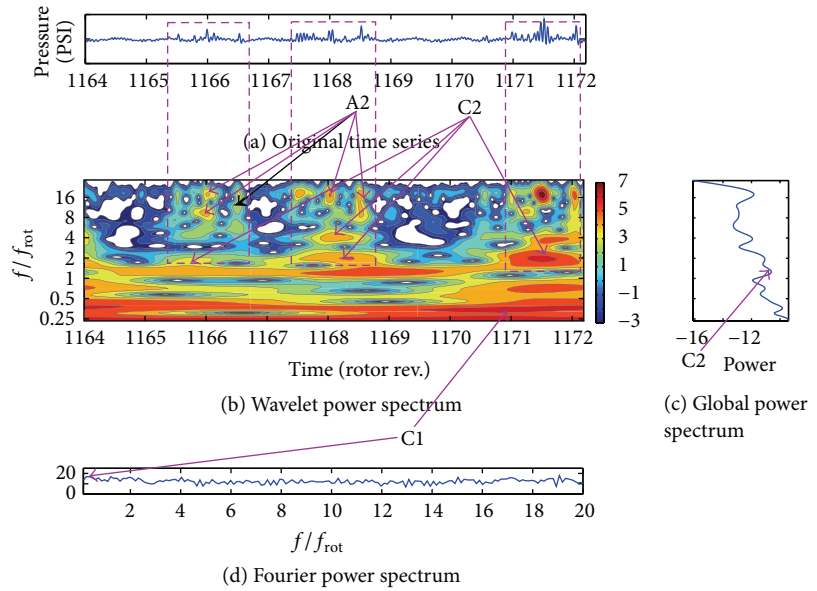

FIGURE 9: Wavelet analysis of data segment for sensor 1 of rotor-1 at stall mass flow (point C) for design speed combination.

length scale disturbance indicated by the dashed rectangles with frequency range of 2 to 8 times the rotor frequency. The LLSDs cover the whole circumference of the fan. The strong modes approximately up to 0.6 times the rotor frequency are observed for all sensors which can easily be seen in Figure 10(b). The two LLSDs observed at sensor 2 are clearly seen in Figure 11 for further clarity and explanation for data segment between 400 and 408 rotor revolutions. Sensor 2 is chosen to show the interval by which the LLSDs occur. In general, it is observed that stall propagation and/or decay for speed combination of 2400–2200 RPM shows that the first stall evolves with a few short length scale disturbances or spikes and within a few rotor revolutions the disturbances transform to long length scale.

Figure 12 shows the casing wall static pressure traces and the corresponding wavelet spectra of all the four sensors data segments of 1192 to 1200 rotor revolutions for speed combinations of 2400–2600 RPM. It is observed that the first stall cell is observed after 1192 rotor revolutions and this indicates that there is a long duration between the starting of the fan and the first instance of stall evolution. The other interesting observation is that the long length scale disturbance evolved at sensor 2 and sensor 4 and decays immediately after the first stall cell. The strong suction effect created by higher rotation of the second rotor helped the fan to restore its stability within a very short period of time of stall initiation.

For further understanding of the condition of the long length scale disturbance, the stall cell for the same data

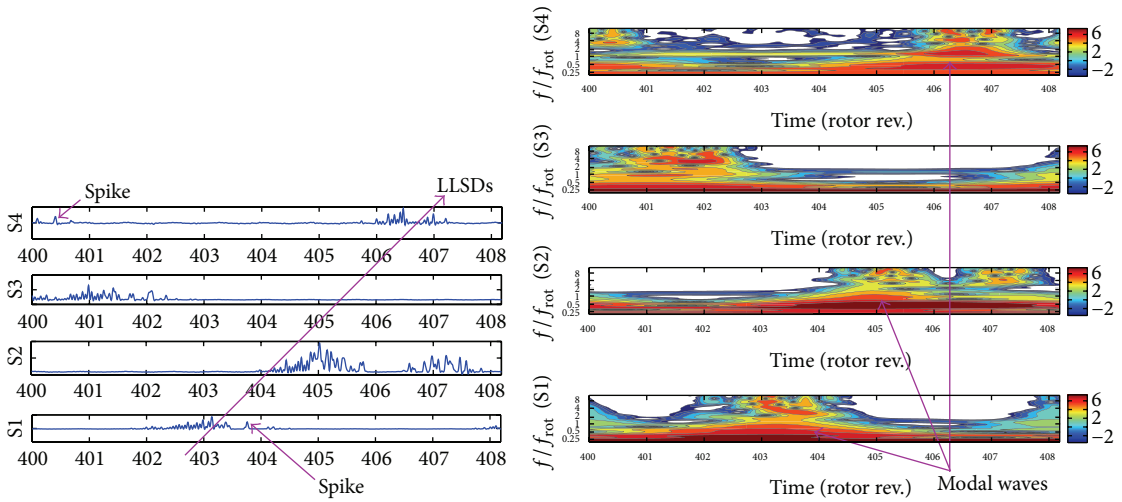

(a) Original time series (b) Wavelet power spectrum

Figure 10: Wavelet analysis of all four sensors of rotor-1 at stall mass flow (point C) for speed combination of 2400–2200 RPM.

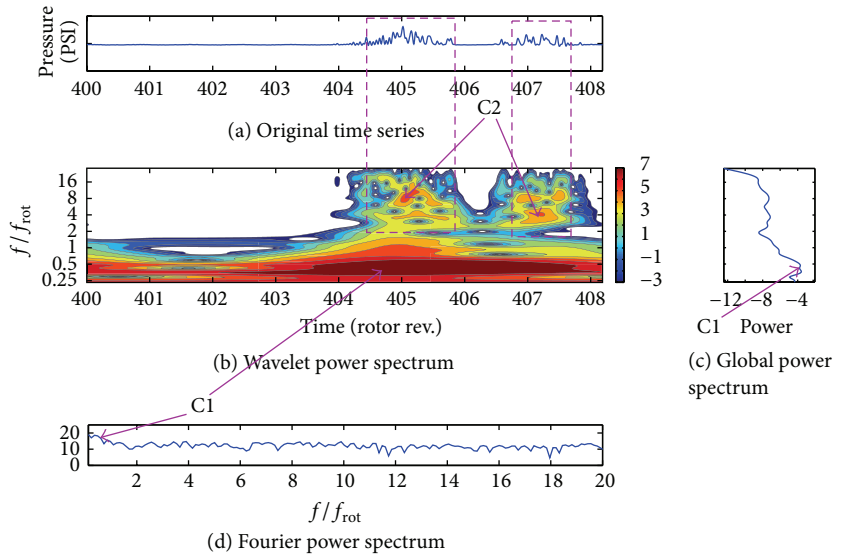

Figure 11: Wavelet analysis of data segment for sensor 2 of rotor-1 at stall mass flow (point C) for speed combination of 2400–2200 RPM.

segment of the case in Figure 12 is analyzed in Figure 13 by considering data from sensor 2. It can be seen that the LLSD stall cell with high energy level covers 2 to 8 times the rotor frequency range. The strong modal waves with frequency of 0.25 to 8 times more than the rotor frequency are also indicated in the wavelet and Fourier power spectrum. This strong mode with higher energy level is also shown in the global power spectrum of Figure 13(d).

5. Stall Inception Study of Rotor-2

The stability of rotor-2 is directly affected by the wake of the forward rotor. Recently, researchers have tried to explore the stall behavior of the downstream rotor. For example, Gao et al. [21] did numerical investigation on the stall inception of the downstream rotor of a contra rotating axial flow compressor. In the present study, four sensors are located circumferentially at 10 mm upstream the leading edge of rotor-2 and data captured according to the procedure given in Section 3.

5.1. Design Mass Flow Condition. The wavelet transforms of unsteady data of casing wall static pressure of rotor-2 at design mass flow and design speed combination are shown in Figure 14. It is intended to show how the rotor behaves at design mass flow or far from stall mass flow. Shaft order perturbations are seen at design mass flow condition and this type of disturbances present almost at all compressors is caused due to nonuniform tip clearance and eccentricity of the rotor and the casing.

5.2. Near Stall Mass Flow Condition. Unsteady raw data of the casing wall static pressure at the peak (near stall) mass

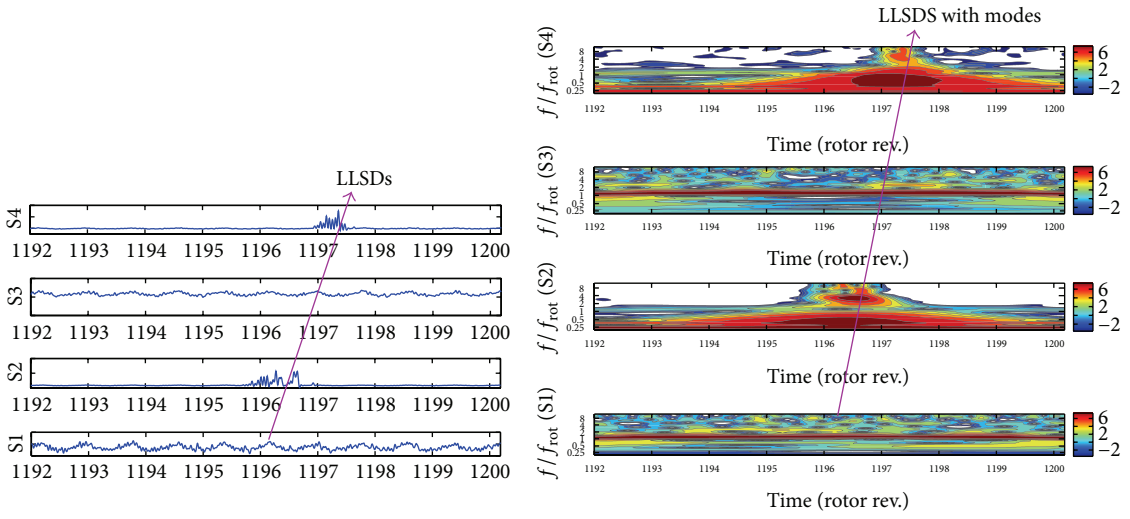

(a) Original time series (b) Wavelet power spectrum

FIGURE 12: Wavelet analysis of all four sensors of rotor-1 at stall mass flow (point C) for speed combination of 2400–2600 RPM.

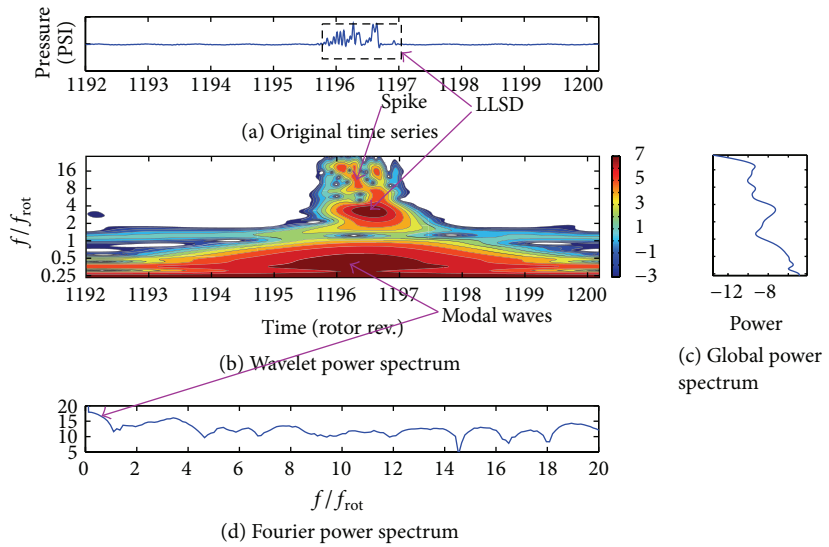

FIGURE 13: Wavelet analysis of data segment for sensor 2 of rotor-1 at stall mass flow (point C) for speed combination of 2400–2600 RPM.

flow condition for design and off-design speed combinations are analyzed by wavelet transforms and are presented in the subsequent sections.

The original time series data of the casing wall static pressure traces and the corresponding wavelet power spectrums of all the four sensors located near the leading edge of rotor-2 are given in Figures 15 and 16 for the design and the off-design speed combinations. In both cases, the stall inception occurs through long length scale disturbance with low energy spots. A marginal increase in the energy level in the wavelet power spectrum is observed in case of 2400–2600 RPM speed combination. For better understanding of the stall phenomena, Figure 17 depicts the pressure traces from one of the sensors. The modal wave indicated in Figure 17(b) shows that it initially propagates with 0.25 times of the rotor frequency and diminishes subsequently. The energy spot and the frequency level increase further (around 0.5 times the rotor frequency). A relatively strong energy spot of blade passing frequency (equal to 16 times frequency of rotor rotation) is also observed. Between the rotor frequency and the blade passing frequency, the energy strength is low which indicates the presence of mild disturbance.

5.3. Stall Mass Flow Condition. By adjusting the throttle position to the same as that of stall mass flow used for rotor-1, unsteady pressure data is captured from the four sensors located near the leading of rotor-2 and wavelet analysis is performed.

The wavelet analysis of the unsteady wall static pressure data obtained from sensor 2 is shown in Figure 18. A mild modal wave, which rotates below 0.25 times the rotor frequency, is observed in Figure 18(b) and the LLSDs with low

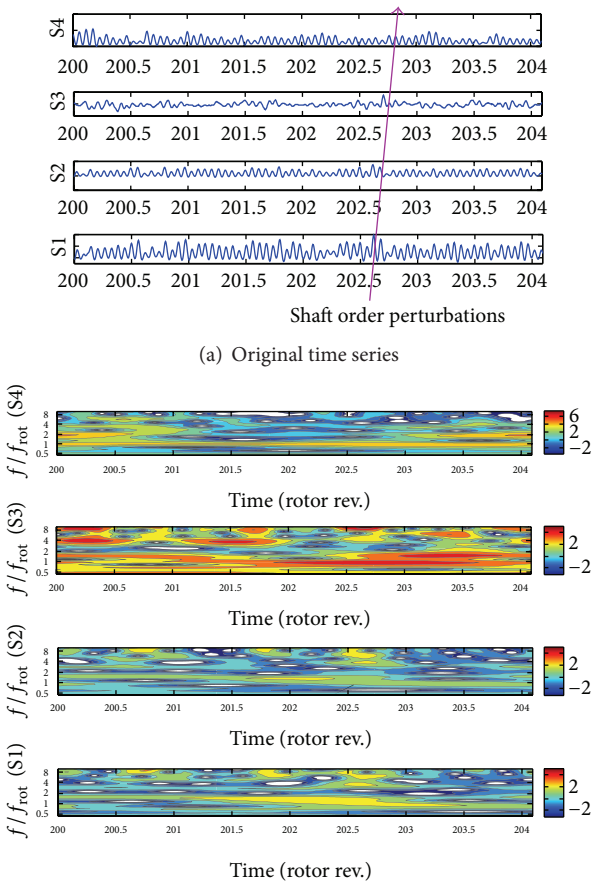

(a) Original time series

(b) Wavelet power spectrum

FIGURE 14: Wavelet analysis of all four sensors of rotor-2 at design mass flow (point A) for design speed combination.

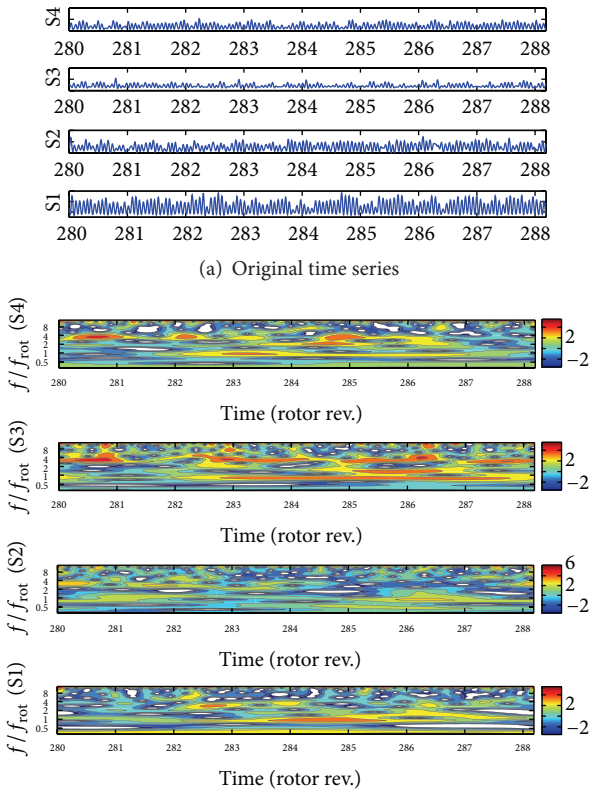

(a) Original time series

(b) Wavelet power spectrum

FIGURE 15: Wavelet analysis of all four sensors of rotor-2 at near stall mass flow (point B) for design speed combination.

energy level are observed between 366 and 372 rotor revolutions with frequency 0.5 to 2 times the rotor frequency. A relatively large amplitude and wavelet energy spot blade passing frequency disturbance are observed in this case. In general, the stall magnitude of rotor-2 is weak compared to rotor-1 at the same throttle level of the stall mass flow condition. This result agrees with the numerical simulation result obtained by Wang et al. [24], where it is stated that the upstream rotor performance is affected more significantly than the downstream rotor for large tip clearance gap of the stage.

6. Additional Discussions

The present paper discusses the stall inception phenomena under clean flow condition for design and off-design speed combinations. It is intended to understand the stall evolution and progress of the contra rotating fan stage for a relatively large tip gap. The investigation has shown some interesting results of the stall inception phenomena. For both design and off-design speed combinations at near stall mass flow of rotor-1, the stall occurs mainly through long length scale disturbances (LLSDs) and short length scale disturbance appears at the initial stage of the disturbance and intermittently. Similar types of stall patterns of stall inception, which combines spike and modal disturbance, were captured by Day [5]. Here, the basic difference is that the LLSDs are the dominant type of stall evolution. The presence of long length scale modal waves was also reported by Nishioka [26] for low stagger axial flow fan with relatively large tip clearance. This phenomenon is shown in Figure 19 and the larger size dashed rectangle shows LLSDs and the smaller size dashed rectangle shows the SLSDs, respectively.

The long length scale disturbance occurred in the case of off-design operation of 2400–2200 RPM triggers to full stall. This disturbance progresses for long durations resulting in unstable operation of the stage. This phenomenon is shown in Figure 20. This result confirms that operating the CRAF stage with lower rotational speed of the second rotor compared to the first rotor decreases the overall performance which was reported in the parametric study of performance of CRAF stage by Mistry and Pradeep [2]. Another interesting important thing observed in the present investigation is that all the disturbances (LLSDs and SLSDs) occurring during stall onset have low amplitude of frequency. This can be seen from Fourier power spectrum in which FFT amplitude is in log2 scale.

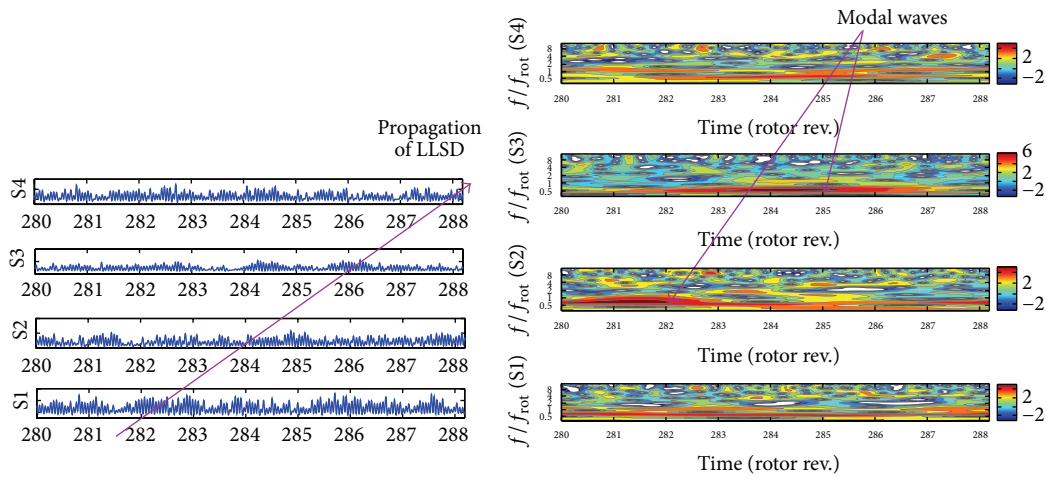

(a) Original time series (b) Wavelet power spectrum

FIGURE 16: Wavelet analysis of all four sensors of rotor-2 at near stall mass flow (point B) for speed combination of 2400–2600 RPM.

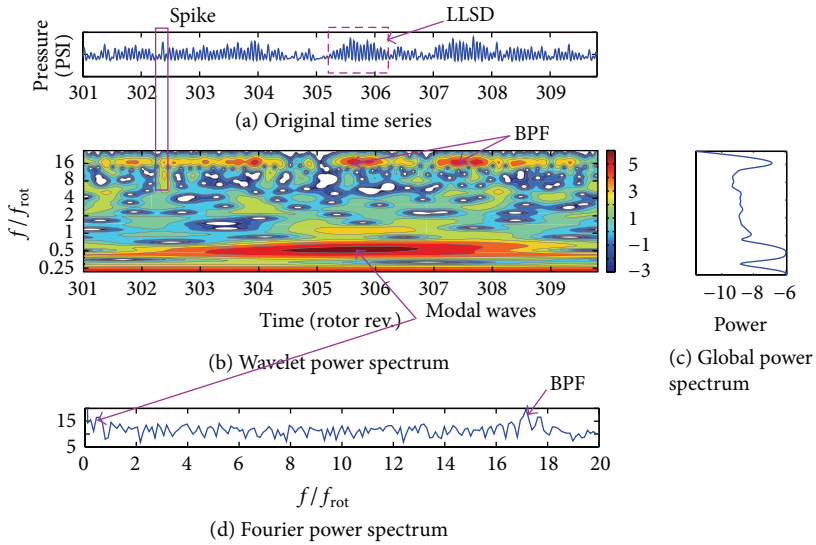

FIGURE 17: Wavelet analysis of data segment for sensor 3 of rotor-2 at near stall mass flow (point B) for speed combination of 2400–2600 RPM.

7. Conclusions

This study explores the stall inception mechanism in a low speed contra rotating axial fan stage with relatively large tip gap. Different operating conditions such as near stall and stall mass flow conditions under different speed combinations were used. Four unsteady pressure sensors were located circumferentially near leading edge of rotor-1 and rotor-2. The growth/decay of disturbances and the route to stall inception are analyzed using 1D continuous Morlet wavelet transform. The major findings of the present paper are given as follows:

(1) Stall inception occurs mainly through long length scale disturbances for both rotors and short length disturbances occur simultaneously and intermittently in case of rotor-1. The existence of spike of disturbance with higher amplitude and frequency within the LLSDs is the unique behavior of the stall phenomena observed in the present investigation. High blade loading (from 60% blade span to the tip section) imposed during the design stage that reaches its maximum limit at the stall mass flow is responsible for the stall initiation.

(2) A strong modal wave is observed in the case of rotor-1 and it was seen for all the speed combinations at the stall mass flow condition. The frequencies at which the modal wave propagates differ for different speed combinations. For design speed combination, modal waves were 25% to 50% of the rotor frequency and for off-design speed combination of 2400–2600 RPM the modal wave propagates with 25% to 80% of the rotor frequency.

(3) The most interesting observation for speed combination of 2400–2600 RPM is that even though the

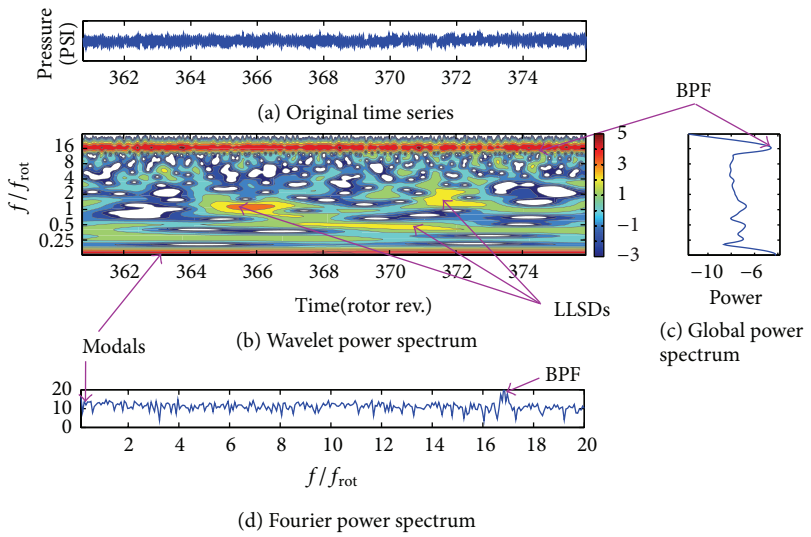

Figure 18: Wavelet analysis of data segment for sensor 2 of rotor-2 at stall mass flow (point C) for speed combination of 2400–2200 RPM.

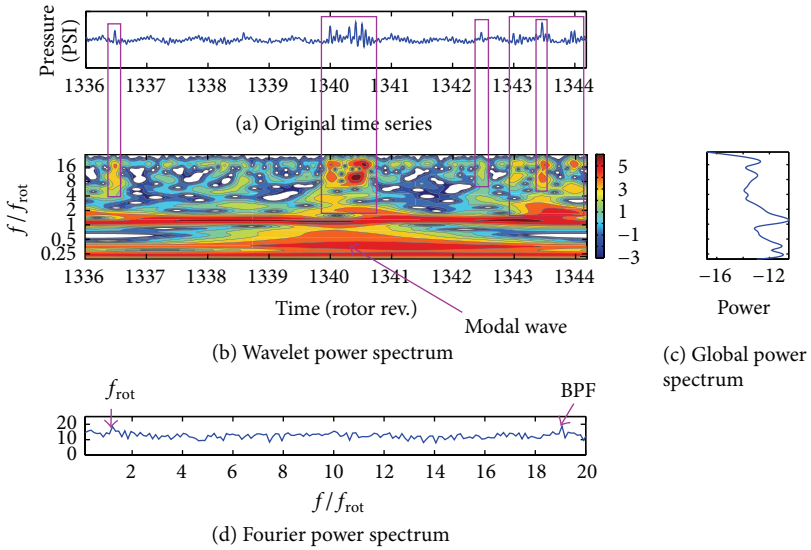

Figure 19: Wavelet analysis of data segment for sensor 1 of rotor-1 at stall mass flow (point C) for design speed combination.

modal disturbance frequency and the wavelet energy strength are higher, rotor-1 restores its stability after short period of stall occurrence due to the strong suction effect created by higher rotation of rotor-2.

(4) In the case of 2400–2200 RPM speeds combination, the long length disturbance observed in rotor-1 triggers to the full stall at stall mass flow condition.

(5) Modal activity observed in the case of rotor-2 is insignificant compared to the case in rotor-1. The modal wave frequency with less than 25% of the rotor frequency and low strength wavelet energy spot is observed in this case. The peculiarity in case of rotor-2 which is relatively a strong wavelet energy blade passing frequency disturbance is observed.

Nomenclature

f: Frequency, rad/s
k: Frequency index
N: Total number of points
P: Total pressure, N/m^2
s: Scale, second
S: Sensor
x: Time series
W: Wavelet coefficient.

Abbreviations

BPF: Blade passing frequency
FFT: Fast Fourier transform
LLSD: Long length scale disturbance
SLSD: Short length scale disturbance.

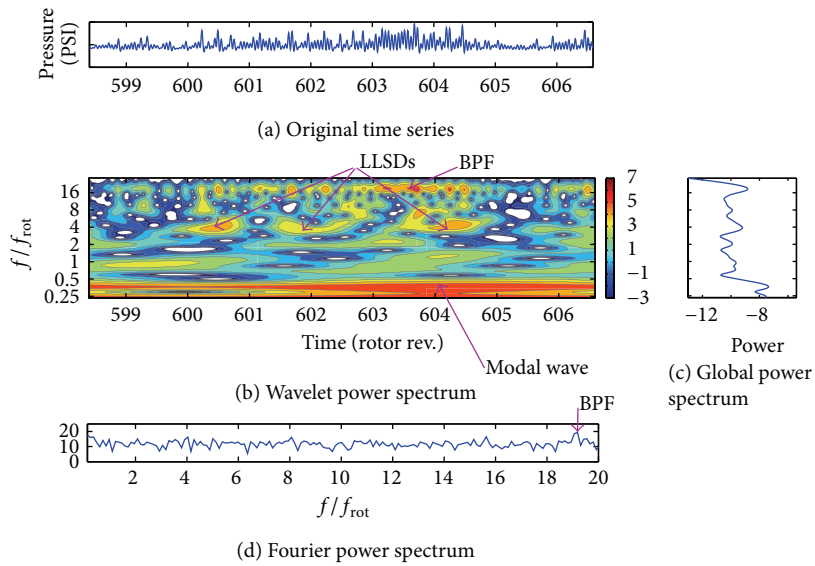

FIGURE 20: Wavelet analysis of data segment for sensor 1 of rotor-1 at stall mass flow (point C) for speed combination of 2400–2200 RPM.

Greek Symbols

η: Nondimensional time
ω_k: Angular frequency corresponding to the frequency index, rad/sec.

Subscripts

01: Rotor-1 inlet
02: Rotor-2 exit
rot: Rotor.

Conflict of Interests

The authors declare that there is no conflict of interests regarding the publication of this paper.

References

[1] H. Nouri, A. Danlos, F. Ravelet, F. Bakir, and C. Sarraf, "Experimental study of the instationary flow between two ducted counter-rotating rotors," *Journal of Engineering for Gas Turbines and Power*, vol. 135, no. 2, Article ID 22601, pp. 22601–22608, 2013.

[2] C. S. Mistry and A. M. Pradeep, "Effect of variation in axial spacing and rotor speed combinations on the performance of a high aspect ratio contra-rotating axial fan stage," *Proceedings of the Institution of Mechanical Engineers, Part A: Journal of Power and Energy*, vol. 227, no. 2, pp. 138–146, 2013.

[3] D. S. Pundir and P. B. Sharma, "A study of aerodynamic performance of a contra-rotating axial compressor stage," *Defence Science Journal*, vol. 42, no. 3, pp. 191–199, 1992.

[4] B. Roy, K. Ravibabu, P. Srinivasa Rao, S. Basu, A. Raju, and P. N. Murthy, "Flow studies in ducted twin-rotor contra rotating axial flow fans," in *Proceedings of the International Gas Turbine and Aero Engine Congress and Exposition*, Paper no. 92-GT-390, pp. 1–8, Cologne, Germany, 1992.

[5] I. J. Day, "Stall inception in axial flow compressors," *Journal of Turbomachinery*, vol. 115, no. 1, pp. 1–9, 1993.

[6] N. M. McDougall, N. A. Cumpsty, and T. P. Hynes, "Stall inception in axial compressors," *Journal of Turbomachinery—ASME Transactions*, vol. 112, no. 1, pp. 116–125, 1990.

[7] P. Kumar and B. Roy, "Using waves to simulate distortion in internal flows in an axial flow fan," in *Proceedings of the 29th Congress of the International Council of the Aeronautical Sciences (ICAS '14)*, pp. 1–10, Saint Petersburg, Russia, September 2014.

[8] T. R. Camp and I. J. Day, "A study of spike and modal stall phenomena in a low speed axial compressor," *Journal of Turbomachinery*, vol. 120, no. 3, pp. 393–401, 1998.

[9] H. D. Vo, C. S. Tan, and E. M. Greitzer, "Criteria for spike initiated rotating stall," *Journal of Turbomachinery*, vol. 130, no. 1, Article ID 011023, 9 pages, 2008.

[10] R. Taghavi-Zenouz and S. Abbasi, "Multiple spike stall cells in low speed axial compressor rotor blade row," *Journal of Theoretical and Applied Mechanics*, vol. 53, no. 1, pp. 47–57, 2015.

[11] J. Pismenny and Y. Levy, "Simultaneous spike-type and modal-type stall inception: theoretical analysis," *International Journal of Mechanical Engineering and Automation*, vol. 1, no. 3, pp. 129–139, 2015.

[12] F. Lin, J. Chen, and L. Meilin, "Wavelet analysis of rotor-tip disturbances in an axial-flow compressor," *Journal of Propulsion and Power*, vol. 20, no. 2, pp. 319–334, 2004.

[13] I. J. Day, T. Breuer, J. Escuret, M. Cherrett, and A. Wilson, "Stall inception and the prospects for active control in four high-speed compressors," *Journal of Turbomachinery*, vol. 121, no. 1, pp. 18–27, 1999.

[14] X. He, H. Ma, J. Zhang, and W. Wei, "Wavelet analysis of the shaft order perturbation and stall inception in an axial compressor," *Journal of Thermal Science*, vol. 22, no. 3, pp. 223–228, 2013.

[15] J. D. Cameron and S. C. Morris, "Analysis of axial compressor stall inception using unsteady casing pressure measurements," *Journal of Turbomachinery*, vol. 135, no. 2, Article ID 021036, 2012.

[16] F. Lin, M. Li, and J. Chen, "Long-to-short length-scale transition: a stall inception phenomenon in an axial compressor with inlet distortion," *Journal of Turbomachinery*, vol. 128, no. 1, pp. 130–140, 2006.

[17] M. Ziach, M. Majkut, and A. Witkowski, "Application of the wavelet transform of pressure signals for detecting and analyzing rotating stall inception in axial flow low speed compressor stage," *Archive of Mechanical Engineering*, vol. 58, no. 1, pp. 61–77, 2011.

[18] P. B. Salunkhe and A. M. Pradeep, "Stall inception mechanism in an axial flow fan under clean and distorted inflows," *Journal of Fluids Engineering*, vol. 132, no. 12, Article ID 121102, 14 pages, 2010.

[19] P. B. Sharma, Y. P. Jain, N. K. Jha, and B. B. Khanna, "Stalling behavior of a contra-rotating axial compressor stage," in *Proceedings of the 7th International Symposium on Airbreathing Engines Conference (ISABE '85)*, Paper no. ISABE 85-7087, Beijing, China, 1985.

[20] Z. Wang, W. Yuan, Q. Li, and Y. Lu, "Experimental investigation on the stall inception of a counter rotating compressor," in *Proceedings of the 2012 ASME Turbo Expo*, Paper No. GT2012-68235, Copenhagen, Denmark, June 2012.

[21] L. Gao, R. Li, F. Miao, and Y. Cai, "Unsteady investigation on tip flow field and rotating stall in counter-rotating axial compressor," *Journal of Engineering for Gas Turbines and Power*, vol. 137, no. 7, Article ID 072603, 2015.

[22] C. Torrence and G. P. Compo, "A practical guide to wavelet analysis," *Bulletin of the American Meteorological Society*, vol. 79, no. 1, pp. 61–78, 1998.

[23] M. Farge, "Wavelet transforms and their applications to turbulence," *Annual Review of Fluid Mechanics*, vol. 24, no. 1, pp. 395–458, 1992.

[24] Y. Wang, W. Chen, C. Wu, and S. Ren, "Effects of tip clearance size on the performance and tip leakage vortex in dual-rows counter-rotating compressor," *Proceedings of the Institution of Mechanical Engineers Part G: Journal of Aerospace Engineering*, vol. 229, no. 11, pp. 1953–1965, 2015.

[25] M. Choi, M. Vahdati, and M. Imregun, "Effects of fan speed on rotating stall inception and recovery," *Journal of Turbomachinery*, vol. 133, no. 4, Article ID 041013, 8 pages, 2011.

[26] T. Nishioka, "Inception mechanism and suppression of rotating stall in an axial-flow fan," in *Proceedings of the 6th International Conference on Pumps and Fans with Compressors and Wind Turbines (ICPF '13)*, vol. 52 of *IOP Conference Series: Materials Science and Engineering*, pp. 1–10, Beijing, China, September 2013.